Aeolian Research 3 (2012) 467–476

Contents lists available at ScienceDirect

Aeolian Research

journal homepage: www.elsevier.com/locate/aeolia

Calibration of RWEQ in a patchy landscape; a first step towards a regional scale wind erosion model

Feras Youssef [a,e,*], Saskia Visser [a], Derek Karssenberg [b], Adriana Bruggeman [c,d], Günay Erpul [e]

[a] Land Degradation and Development Group, Wageningen University, P.O. Box 47, 6700 AA Wageningen, The Netherlands
[b] Department of Physical Geography, Faculty of Geosciences, Utrecht University, P.O. Box 80115, 3508 TC Utrecht, The Netherlands
[c] International Center for Agricultural Research in the Dry Areas (ICARDA), P.O. Box 5466, Aleppo, Syria
[d] Energy, Environment and Water Research Center, CREF/The Cyprus Institute, P.O. Box 27456, 1645 Nicosia, Cyprus
[e] Soil Science Department, Faculty of Agriculture, University of Ankara, Soil Science Department, P.O. Box 06110, Dışkapı Ankara, Turkey

ARTICLE INFO

Article history:
Available online 13 April 2011

Keywords:
Wind erosion modelling
RWEQ
Syria
Regional scale
Soil loss

ABSTRACT

Despite the fact that wind erosion seriously affects the sustainable use of land in a large part of the world, validated wind erosion model that predicts windblown mass transport on a regional scale is lacking. The objectives of this research were to modify revised wind erosion equation (RWEQ) to estimate soil loss at a field scale in a way that it could operate at a regional scale, to calibrate the model using ground data collected from a field scale representing different land uses in Khanasser valley, Syria, and to estimate the total sediment fluxes (kg m^{-1}) and soil losses (kg m^{-2}) for farming fields.

We implemented a modified version of RWEQ that represents wind erosion as a transient process, using time steps of 6 h. Beside this a number of adaptations including estimation of mass flux over the field boundaries, and the routing of sediment have been done. Originally, RWEQ was created and calibrated for application at the scale in USA. Due to the adaptations imparted to the original RWEQ and the different environmental condition in Syria of application areas, an intensive calibration process was required before applying the model to estimate the net soil loss from the experimental fields.

The results of this test showed that the modified version of RWEQ provided acceptable predictions for the average mass flux from the measurement plot with a linear regression coefficient of R^2 of 0.57 and 0.83 for the (d) test for the 20 wind events at the six tested plots.

1. Introduction

Wind erosion is an important problem in arid and semi-arid regions (Buschiazzo and Zobeck, 2008; Stroosnijder, 2007). Wind erosion significantly decreases soil productivity (Sterk et al., 1996; Visser and Sterk, 2007) and has negative effects on human health due to the harmful effects of dust particles on the respiratory system (Copeland et al., 2009; De Longueville et al., 2009). When conditions favorable for wind erosion are present, the process may result in large scale environmental disasters like the Dust Bowl in the USA in the 1930s, which affected more than 40 million hectares of lands (Cook et al., 2008). The amount of soil loss by wind erosion is mainly determined by meteorological conditions, vegetation cover, land management and soil properties (Leenders et al., 2005; Sterk and Spaan, 1997).

Minimizing soil loss is essential to reduce land degradation and to optimize crop yields. Thus, in regions that are vulnerable to wind erosion, prediction of soil loss at the regional scale is an important step in designing land use plans (Feng and Sharratt, 2007; Papadimitriou and Mairota, 1996). Despite this critical need for regional scale prediction of wind erosion, a limited number of regional scale models exist. In addition, most existing regional scale wind erosion models have not been calibrated and validated against the data of ground observations collected at a regional scale (Shao and Leslie, 1997; Zobeck et al., 2000). Therefore, regional scale wind erosion models and field sampling schemes are needed specifically at the regional scale. Clearly, there is a need for models that can run with data available at the regional scale. Regional data generally consist of maps or remotely sensed information of land use, vegetation cover and soil type with resolution above 100 m. Thus, regional scale models should have size units comparable to an arable field (100–10,000 m^2) with model equations for each unit that can be solved using limited attribute information. Such models could then predict soil loss for each arable field (i.e., model unit), taking into account properties of the field itself and the spatial configuration of neighboring fields. Regional

* Corresponding author at: Land Degradation and Development Group, Wageningen University, P.O. Box 47, 6700 AA Wageningen, The Netherlands.
E-mail addresses: feras.youssef@wur.nl (F. Youssef), Saskia.visser@wur.nl (S. Visser), d.karssenberg@geo.uu.nl (D. Karssenberg), a.bruggeman@cyi.ac.cy (A. Bruggeman), Gunay.Erpul@agri.ankara.edu.tr (G. Erpul).

1875-9637/$ - see front matter © 2011 Elsevier B.V. All rights reserved.
doi:10.1016/j.aeolia.2011.03.009

scale modelling cannot be supported by real-time observations of mass transport or soil loss as it is infeasible to design and maintain sampling schemes that monitor wind erosion at the regional scale with models that are properly calibrated. To do so, field sampling schemes specifically directed towards calibration of (components of) regional scale models are required.

To cope with these challenges, we describe a methodology which combines modelling and field sampling efforts together. Thusly, the objectives of this research are (1) to adjust an existing wind erosion model capable to predict soil loss at the scale of a field such that it could perform at a regional scale, using limited input data, (2) to calibrate the model against observations from a field monitoring scheme particularly designed for calibration of regional scale models with a size of model units comparable to arable fields and (3) to calculate total sediment fluxes (kg m^{-2}) (loss or deposition) for arable fields. In this modelling work, the existing RWEQ model (Fryrear et al., 1998) was used as a starting point as it needs limited input data compared to mechanistic wind erosion models such as wind erosion prediction system (WEPS) (Hagen, 2004). The RWEQ model was adjusted to prepare the model for simulation at the regional scale. RWEQ was translated into PCRaster to enable simulation of spatial variation in vegetation cover and eroding boundaries. Furthermore, the model was modified to take advantage of standard meteorological time series data by using transient temporal simulations. Also, net wind erosion over arable fields was calculated, which is essential for regional scale modelling. Key model parameters were found by an extensive brute force calibration technique using a new data set collected at six arable fields in the Khanasser region, Syria.

2. Materials and methods

2.1. Study area

The Khanasser valley is situated between the Al Hass and Shbeith mountains (Fig. 1), southeast of Aleppo city, Syria. At an altitude of 350 m above sea level, the valley is rather flat. Annual rainfall ranges from 150 to 250 mm and the rainy season starts in October and ends in May (Masri et al., 2003). Wind in the dry season (from June to September) travels from south to west with exceptional large wind events from other directions. During the dry season, the daily average wind speed (at 2 m height) is high and may exceed 10 m s^{-1} (Masri et al., 2003). Monthly average wind speed in the valley varies from 3.5 m s^{-1} in the south up to 4.4 m s^{-1} in the north (Bruggeman et al., 2008).

Calcisols, Gypsisols, Leptisols, and Cambisols are the main soil types in the valley (Masri et al., 2003). These soils are well-drained and have clay-loam to sandy-loam texture. The intensive agricultural and livestock activities and poor management of limited natural resources are dominant problems in the valley. These land use conditions resulted in a significant increase in the land degradation in the valley (ICARDA, 2005).

Wind erosion is one of the most dominant land degradation problems threatening not only the agricultural and livestock activities but also the settlements in the valley (Thomas and Turkelboom, 2008). According to the annual rainfall, Syria can be divided into five stability zones. In stability zone 4, the annual rainfall is 200–250 mm and the main land use is dry farming (mainly cereals). In stability zone 5, the annual rainfall is less than 200 mm and the land use varies from pastures to rangelands where cultivation activities are currently prohibited. This research is carried out in stability zones 4 and 5 in Khanasser valley. In zone 4, the agricultural fields were divided equally among farmers in a way that all fields have access to the small number of roads which are oriented north–south. As a result of this division the fields are 50–80 m in width and 2000–4000 m in length in the east–west direction. The plough direction follows the field direction (east–west) in order to reduce the cost and time of ploughing activities. The research was carried out using a "portable" plot approach, to allow for a number of different locations to be handled with a relatively small set of equipments. For this research data from six measurement plots were used (Table 1). No special treatments

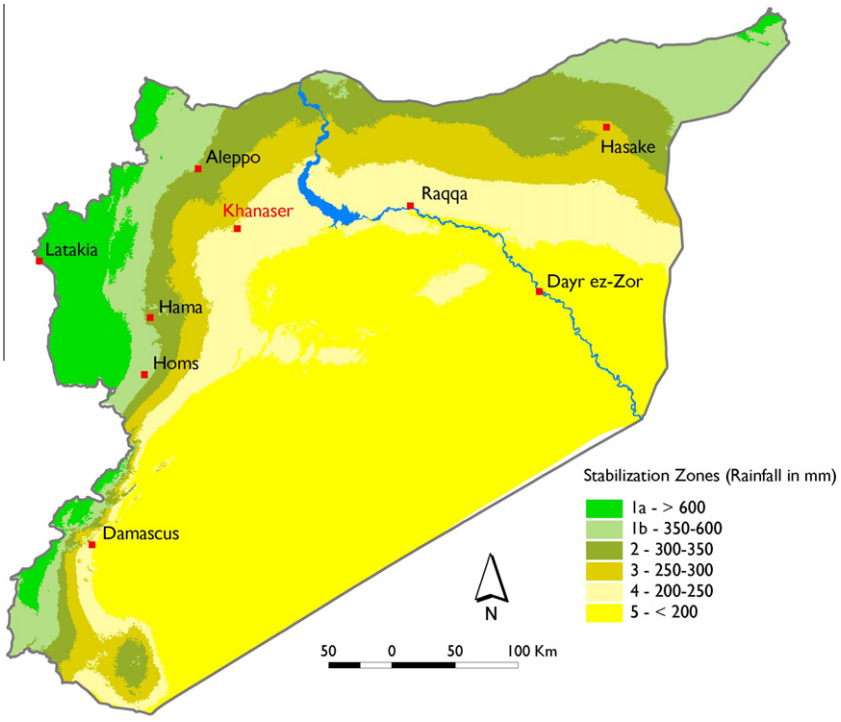

Fig. 1. The location of Khanasser valley, and the stability zones in Syria (ICARDA, 2005).

Table 1
Description of the wind erosion measurement plots with their zones, crops, soil textures and land uses in the Khanasser valley, Syria.

Name of plot	Zone	Crop	Soil[a]	Land use
Serdah A	4	Wheat	Clay-loam	Harvested field with partially grazing; standing silhouette
Serdah C	4	Camion	Clay-loam	Harvested field with Intensive grazing, no standing silhouette
Mugherat A	4	Wheat with Atriplex	Sandy-loam	Harvested field with Intensive grazing, no standing silhouette, shrubs of Atriplex
Mugherat NA	4	Wheat	Sandy-loam	Harvested field with Intensive grazing, no standing silhouette
Um Mial	4	Barley	Clay-loam	Harvested field with Intensive grazing, no standing silhouette
Adami Gazelle	5	Atriplex reserve	Silt-loam	Reserve area with Atriplex with partial grazing

[a] Soil type was determined with the Soil Texture Calculator (NRCS, 2010).

on the surface of the measurement plots were applied before or during the measurement periods. Furthermore, most plots did not obtain a non-eroding boundary. Consequently, sediment could freely blow into and out of the plot without obstructions.

Between June and September 2009, measurements on vegetation characteristics, soil parameters, climate and wind-blown mass fluxes were taken to evaluate wind erosion for a period of three weeks per field. After each three periods the research set up was broken down and transferred to the next plot. At each site the wind profile was measured using five anemometers gauging wind speeds at 0.40, 1, 1.88, 3.00 and 4.00 m heights. A wind vane recorded wind direction (degrees) as well. A saltiphone (Spaan and van den Abeele, 1991) was used to determine the onset of wind-blown mass transport and the total duration of saltation. Furthermore, the temperature, relative humidity and soil moisture were measured. All sensors were connected to a CR1000 data logger, which stored sensor outputs at 5 min intervals. Information on solar radiation was obtained from measurements performed by ICARDA over long periods (Bruggeman et al., 2008).

Vegetation characteristics (surface coverage, height), soil properties (texture, organic matter and calcium carbonate) and soil surface roughness (ridge spacing, ridge height) were determined at the start of the experiments for each plot. Due to the dry conditions and absence of management activities, it was assumed that values of these parameters did not change during the sampling period. Soil properties were obtained by soil analysis of eight soil samples for each plot in the laboratories of ICARDA. Thus, by analyzing eight soil samples from each plot, the values of soil texture, OM and $CaCO_3$ were obtained using the hydrometer method, the method of Walkley and Black (Walkley and Black., 1934) and the acid neutralization method, respectively. The roughness and the vegetation characteristics were collected through direct field observations. Each plot (60×60) was divided into 144 parcels with (5×5 m) area for each parcel. At each parcel five observations were recorded for the vegetation height, vegetation cover and residues, the random roughness using the chain method (Saleh, 1993) and the oriented roughness.

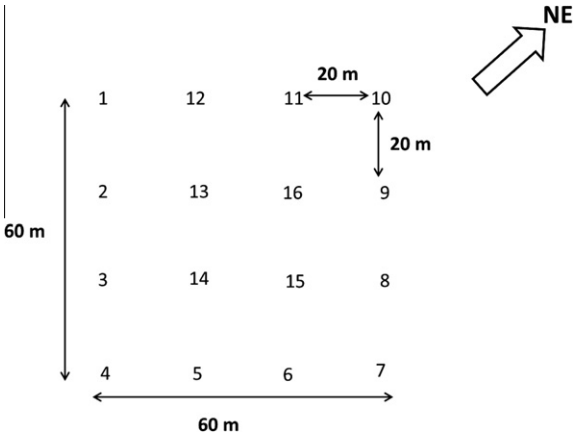

Fig. 2. A sample of a measurement plot with positions of 16 MWAC catchers.

For the measurement of wind-blown sediment fluxes 16 MWAC catchers were set-up in a regular grid on a 60×60 m plot (Fig. 2). This set up of catchers provided a transect of mass fluxes regardless of the wind direction. Furthermore, changes in the flux at the borders of fields were measured in this way because the small size of the plot allowed observation of sediments that blown in or out the plot. Sediments were collected four times at Serdah C and Um Mial and three times at the other plots because of the restriction of the measurement time. The sediment was collected mainly on weekly-based with some exceptions due to some logistical issues during the start of the research. The total mass transport ($kg\,m^{-1}$) was calculated through sampling the horizontal mass fluxes at five heights (0.10, 0.30, 0.50, 0.75 and 1.00 m). Then, the approach of Sterk and Raats (1996) was applied to build up a flux profile by height.

2.2. The revised wind erosion equation

The RWEQ model was developed by Fryrear et al. (1998) in order to estimate soil loss from agricultural fields in the USA. The RWEQ model not only is the best applicable methodology for the prediction of wind erosion at a field scale, but also provides information on erosion rates within the field (Fryrear et al., 1998). This paper only reports the key processes and equations of the RWEQ models, and for a complete description of all model equations the reader is referred to (Fryrear et al., 1998). The RWEQ model makes estimates of sediment eroded and transported by wind between the soil surface and a height of 2 m for specified periods based on a single-event. The temporal interval used in RWEQ is 1–15 days. The simulation area is a homogeneous circular or rectangular field bounded by a non-eroding boundary. The model calculates aeolian mass transport ($Q(z)$; $kg\,m^{-1}$) at downwind distance (Z, m) in the field from the balance between wind erosivity and soil erodibility with:

$$Q(z) = Q_{max} \cdot (1 - e^{\left(\frac{Z}{S}\right)^2}) \quad (1)$$

With, Q_{max} ($kg\,m^{-1}$); the maximum transport capacity and S (m); the critical field length defined as the distance at which the 63% of maximum transport capacity is reached. The erosivity of the wind is expressed in the weather factor (W_F, $kg\,m^{-1}$), which is calculated based on weather related input parameters. The erodibility of the soil is expressed in a crusting factor (C_F), erodible fraction (E_F), a combined crop factor (C_{OG}) and a single roughness factor (K_{tot}) (Fig. 3). The erodibility and erosivity are combined in the calculation of maximum transport capacity (Q_{max}) and the critical field length (S), which are, respectively calculated as:

$$Q_{max} = 109 \cdot (W_F \cdot E_F \cdot S_{CF} \cdot K_{tot} \cdot C_{OG}) \quad (2)$$

$$S = 150.71 \cdot (W_F \cdot E_F \cdot S_{CF} \cdot K_{tot} \cdot C_{OG})^{-0.3711} \quad (3)$$

The average soil loss (S_L; $kg\,m^{-2}$) at a specific point (Z, m) in the field can be computed with:

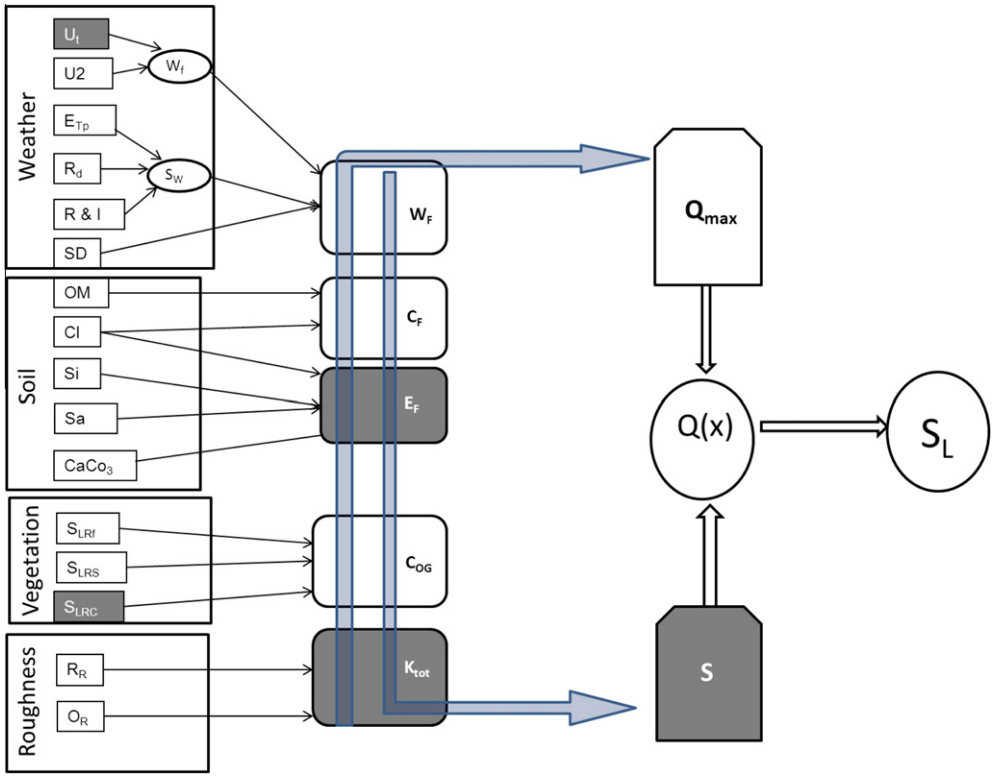

Fig. 3. Illustration of calculation steps for soil loss SL and mass transport $Q(x)$ in RWEQ. U_t, threshold velocity at 2 m height; U_2, wind speed at 2 m; W_f, wind factor; E_{T_p}, potential relative evapotranspiration; R_d, number of rainfall/irrigation days; R&I, rainfall and irrigation; SD, snow depth; S_W, soil moisture; W_F, weather factor; OM, content of organic matter; Si, content of silt; Cl, content of clay; *Sa,* content of sand; $CaCO_3$, calcium carbonate; C_F, crust factor; E_F, erodible fraction; S_{LRf}, flat residue; S_{LRs}, standing residue; S_{LRc}, crop cover; C_{OG}, combined crop factors; R_R, random roughness; O_R, orientated roughness and K_{tot}, single soil roughness factor. The highlighted boxes with white letters include the parameters that were calibrated.

$$S_L = \frac{2 \cdot Z}{S^2} Q_{max} \cdot e^{-\left(\frac{Z}{S}\right)^2} \quad (4)$$

where Z: is the distance from non-erodible border.

2.3. Translation of RWEQ into PCRaster

A major advantage of using RWEQ is that the model is relatively simple and requires a limited amount of input data, which makes the model relatively easy to be scaled up. In the development of RWEQ, the relation between soil loss and field length was determined for homogenous circular or rectangular fields. With the obtained relationship, soil loss from any field shape or size can be evaluated. The model inputs related to vegetation cover and soil roughness vary in temporal scale from daily to bi-weekly averages. Furthermore, the USA climate generator CLIGEN is used to simulate rainfall, wind speed, temperature and evaporation.

For the application of the RWEQ in this research, it is necessary for the model should take into account incoming and outgoing sediment fluxes at the edge of a field, use measured input data for climate parameters and take into account the presence of a non-homogeneous vegetation cover. Furthermore, for the application of the RWEQ at a regional scale the model should be able to simulate mass transport over units with varying vegetation cover and patterns. In its current state the RWEQ does not have the required flexibility and therefore, it was decided to rewrite the RWEQ into the dynamic modelling language of PCRaster (Karssenberg and De Jong, 2005). PCRaster is an environmental modelling language embedded in a Geographical Information System, providing spatial and temporal functions that can be used to construct transient models.

Apart from the translation of the RWEQ to PCRaster, additional adaptations to the model included (1) simulation of transport over the field boundaries and (2) the time step, which allowed to use the model inputs and outputs in a time series format. Thus, at every time step, the model calculated the mass transport depending on weather inputs. As the assumption of the presence of a non-eroding boundary was invalid for the simulation area, it was decided to use the large scale land use map to determine the actual position of an upwind non-eroding boundary and adjust the simulation area such that it included the actual non-eroding boundary. To be able to account for the large variations in wind speed and wind direction within a day during the field measurements, a simulation time step of 6 h was used, dividing a day in four periods, starting at 1–6, 6–1, 12–18 and 18–24 h. The weather factor (W_F) was simulated for each time step separately. Average wind direction for each time step is used to calculate the distance of each grid cell to the upwind border of the plot. With these model adjustments, the model is made capable of calculating and showing mass transport related to the temporary climate variables and spatial field characteristics.

Table 2 shows the range of values to the main inputs of the model for one plot as an example to show the magnitude of the input values of the model.

2.4. Model calibration

Because the RWEQ was developed and calibrated for application at field scale in the USA (Van Pelt et al., 2004), and since this research attempted to significantly adjust it to apply at fields in Syria, the RWEQ in PCRaster required a thorough calibration. As weather, soil, vegetation and roughness are the main factors of the RWEQ

Table 2
The range of values of main input parameters of RWEQ in PCRaster for the Serdah C measurement plot.

Factors	Input parameters	Parameter values
Weather factor (temporal variable)[a]	Wind speed (m s^{-1})	3.00–7.00
	Wind direction (°)	137–252
	Temperature (°C)	23–38
	Solar radiation (Cal/cm^2)	155.00
Soil and erodible factor (spatial variable)	Content of organic matter (%)	1.25–1.55
	Content of clay (%)	15–26
	Content of sand (%)	45–65
	Soil moisture (%)	1.0–4.0
Roughness and crust factor (spatial variable)	Plough ridge spacing (cm)	35–40
	Plough ridge height (cm)	8–10
	Soil roughness (chain method)	1.2–3.5
Vegetation/residues factor (spatial variable)	Covered surface (%)	7–13
	Height of vegetation or silhouette (cm)	2–5

[a] The presented input parameters for the weather factor are the wind events 4–11 and 11–18 August, 2009.

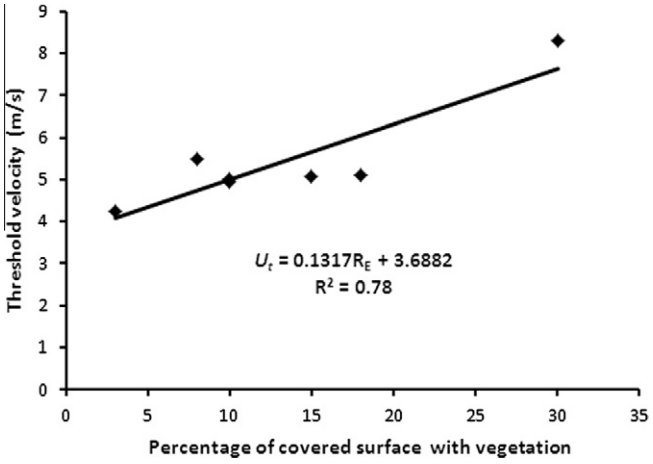

Fig. 4. The relationship between the percentage of vegetation cover, residues and rocks and the threshold wind velocity.

model (Fig. 3), it was decided to use one parameter from each of these factors in the calibration process. Therefore, six calibration parameters, involved in the determination of the critical field length (S, m), the threshold wind velocity (U_t, m s^{-1}), the erodible fraction (E_F), the crop canopy (S_{LRC}) and the soil roughness factor (K_{tot}), were used in this calibration.

For the critical field length (S) the two fixed parameter values used in the original RWEQ model (Fryrear et al., 1998) were replaced by calibration parameters, and S was calculated as:

$$S = \mu_{Sa} \cdot (W_F \cdot E_F \cdot S_{CF} \cdot K_{tot} \cdot C_{OG})^{-\mu_{Sb}} \quad (5)$$

where μ_{Sa} and μ_{Sb} are the parameters of calibration for the critical field length equation. The threshold wind velocity (U_t m s^{-1}) is used in the calculation of the wind value (W_f). Although in the original RWEQ this threshold is considered a constant value, field observations proved that the threshold velocity was related to the percentage of vegetation cover (Fig. 4). The relation given by Eq. 6 was therefore used in the calculation of the threshold velocity in our model

$$U_t = 0.13 \cdot R_E + \mu_{U_t} \quad (6)$$

where R_E is the percentage of the soil surface covered with vegetation and μU_t is a calibration parameter for the threshold velocity.

Depending on the threshold velocity and the wind speed at 2 m height the wind value $(m/s)^3$ is calculated as (Fryrear et al., 1998):

$$W = \sum_{i=1}^{N} U_2 (U_2 - U_t)^2 \quad (7)$$

where U_2 is the wind speed at 2 m height, U_t is the threshold velocity and N is the number of wind speed observations (i) in a time period of 1–15 days in the original version of the RWEQ and 6 h in our adapted version.

The wind factor (W_f, $(m/s)^3$) was calculated as (Fryrear et al., 1998):

$$W_f = \frac{W}{500} \cdot N_d \quad (8)$$

where W is the wind value $(m/s)^3$, N_d is the number of days in the period of measurements (15 days in the original version of the RWEQ and 0.25 day in our adapted version)

The soil erodible fraction (E_F) depends on the soil texture, the content of organic matter and the calcium carbonate ($CaCO_3$) and by including the calibration parameter μE_F, E_F is calculated as (Fryrear et al., 1998):

$$E_F = \frac{\mu E_F + 0.31 S_A + 0.17 S_i + 0.33 \frac{S_A}{C_L} - 2.59 OM - 0.95 CaCO_3}{100} \quad (9)$$

In Eq. 9, S_A is the content of sand (%), S_i is the content of silt (%), C_L is the content of clay (%), OM is the organic matter (%) and $CaCO_3$ is percentage of the calcium carbonate of the soil samples (%).

The crop canopy factor (S_{LRc}) is calculated as a function of the soil that is covered with a crop canopy (C_C), and incorporating the calibration parameter μ_{slrc}, S_{LRc} is calculated as follows (Fryrear et al., 1998):

$$S_{LRc} = e^{-\mu_{Slrc}\left(c_c^{0.7366}\right)} \quad (10)$$

The soil roughness factor is estimated by:

$$K_{tot} = e^{(1.86 \cdot K_{rmod} - 2.41 \cdot K_{rmod}^{0.934} - \mu_{K_{tot}} \cdot C_{rr})} \quad (11)$$

In which K_{rmod} is the modified roughness factor, $\mu_{K_{tot}}$, is the calibration parameter for the roughness factor and C_{rr} is the measured chain roughness (Saleh, 1993).

The model was calibrated against data from all events and plots together. We followed this approach in order to find a single set of parameters that is applicable under a wide range of land use, soil type, and weather conditions. This is essential for application of the model at the regional scale because the range of environmental conditions will be large, and further calibration at the regional scale will not be feasible. We used a brute force technique for calibration. This technique calibrates the model by providing it a wide range of parameter inputs, running it for each parameter set, and

selecting the model run that has a minimum value of the objective function. Here we use the mean square error as objective function, as described below. For each calibration parameter, we selected five different values falling within a range that can be considered physically possible. Then, the calibration was done for all sets of possible combinations of parameter values, resulting in approximately 15×10^3 number of calibration runs. This procedure was iterated a number of times, each time narrowing the range of acceptable parameter values. In the first calibration step, the ranges around the original values used in the RWEQ manual (Fryrear et al., 1998) were used. Then, to reduce the search space the ranges were reduced. The objective function was calculated as follows. First, MSE_i was calculated as:

$$MSE_i = \sum_{n=1}^{n=16} \frac{(Q_{observed,i} - Q_{predicted,i})^2}{16}$$

where $Q_{observed}$ is the measured mass flux of catcher, $Q_{predicted}$ is the predicted total mass flux by the model and the number of 16 is the total number of catchers used in one measurement plot.

Second, the value of MSE_{tot} for all events was determined as:

$$MSE_{tot} = \sum_{i=1}^{i=j} 1 \ldots j(MSE_i) \quad (12)$$

where MSE_i is the mean square error of plot i, with $i = 1,2 \ldots j$, with j the number of plots and events.

2.5. Statistical analysis

The d test (Willmott, 1981), which was also employed by Feng and Sharratt (2007) for testing the (WEPS) model was used to evaluate the model performance. The d value is calculated as:

$$d = 1 - \left[\frac{\sum_{i=1}^{n} (Q_{p_i} - Q_{o_i})^2}{\sum_{i=1}^{n} (|Q_{p_i} - Q_{oM}| + |Q_{o_i} - Q_{oM}|)^2} \right] \quad (13)$$

where Q_p is the predicted value, Q_o is the observed or measured value, n is the number of observation, Q_{oM} is the mean measured value and d ranges from 0 to 1.

3. Results and discussion

3.1. General results of field measurements

The characteristics of the wind events for given time (which was 1 week for most events) and the measured mass fluxes for each event are given in Table 3.

The averages of wind speeds and wind directions varied among the plots and events. The maximum of average wind speed over all events was recorded at the Serdah A measurement plot for the event of 9–30 July. Despite the fact that the main wind direction was WSW for most events, there was an important number of events for which the wind direction was different. For example, at the Adami Gazelle plot ESE and SSW were the main wind directions during the measurement periods. The results of the measured mass flux are not parallel with the wind speed. That is because total mass flux from a field depends not only on weather characteristics but also on vegetation cover, soil properties and soil roughness. Thus, at the Serdah A while the average of wind speed for the event of 9–30 July was 8.77 m s^{-1} which was the highest average speed among all events, the measured mass flux for this event was 1.05 kg m^{-1} which was relatively low compared to higher mass fluxes measured at few other events. On the other hand, the average wind speed during the event of 28–4 August at Um Mial was 4.59 m s^{-1} representing the minimum average wind speed among all events that resulted in 1.6 kg m^{-1} for mass flux, which was relatively higher value comparing with those of other events.

3.2. Results of model calibration

Table 4 shows the original model parameter values, the range used for each parameter, the results of the calibration process and the MSE_{tot}.

The resulted parameters were used in the adjusted model to calculate the spatial mass transport and soil loss over simulated units. Fig. 5 shows an example for the model prediction of the spatial mass (kg m^{-1}) flux for four wind events over the Um Mial measurement plot.

Fig. 5 clearly depicts that the estimated spatial mass fluxes during the four wind events have similar patterns although the values

Table 3
The average of mass fluxes ($Q_{average}$),measured at an event base from six measurement plots.

Site	Date	Dur (hh: min)	WS (ms^{-1})	Wind factor $(m/s)^3$	WD (°)	$Q_{average}$ (kg m^{-1})	$Q'_{average}$ (g cm^{-1} day^{-1})
Serdah A	9–30 July	7:48	8.77	114.81	WSW	1.05	0.500
	30 July–6 August	9:25	6.86	386.39	WSW	0.67	0.957
	6-13 August	1:37	7.02	12.32	WSW	1.21	1.729
Serdah C	16–28 July	2:36	6.86	177.49	WSW	1.88	1.567
	28 July–4 August	2:00	7.86	132.59	WSW	1.04	1.486
	4–11 August	1:34	6.97	53.03	WNW	0.74	1.057
	11–18 August	0:21	6.89	30.72	WSW	1.04	1.486
Mugherat A	13–20 August	1:58	5.64	16.95	SSW	0.50	0.714
	20–27 August	3:50	5.83	25.41	SSW	8.60	12.286
	27August–3 September	11:50	6.23	102.76	SSW	10.54	15.057
Mugherat NA[a]	3–10 September	13:45	6.57	126.36	SSW	3.47	4.957
	10–18 September	2:20	5.42	13.89	NNE	3.57	5.100
	18–25 September	2:30	5.61	9.12	ESE	2.33	3.329
Um Mial	16–28 July	18:10	4.86	83.06	WSW	4.75	3.958
	28–4 August	1.43	4.59	65.70	WSW	1.60	2.286
	4–11 August	2:06	6.99	31.51	WSW	0.59	0.843
	11–19 August	0:58	6.95	23.73	WSW	1.12	1.600
Adami Gazelle	9–16 September	17:0	6.88	42.30	ESE	3.49	4.986
	16–23 September	8:50	6.24	26.55	ESE	3.59	5.129
	23–30 September	21:3	5.25	6.15	SSW	0.69	0.986

[a] Duration; WS, average wind speed during each wind event; WD, average wind direction during each wind event; $Q_{average}$, the average of total mass flux (kg m^{-1}) and $Q'_{average}$ the average of mass flux (g cm^{-1} day^{-1}).

Table 4
The results of calibration together with the original parameters (Fryrear et al., 1998) and their ranges from the 20 events totally observed in six plots.

Parameters	Original values	Range tested	Calibration results	MSE_{tot}
μ_{Sa}	150.71	100–350	300	208.3
μ_{Sb}	0.3711	0.03–0.17	0.03	
μ_{Ut}	–	3–4.2	3	
μ_{EF}	29.09	4–14	6	
μ_{SLRC}	5.614	1.2–2.7	1.7	
$\mu_{K_{tot}}$	0.124	0.03–0.11	0.03	

of mass fluxes varied from one event to another. The similarity in the patterns of spatial mass fluxes resulted from the dominant wind direction during the measurement period, which was WSW (Table 3), while the differences between mass fluxes values stemmed from the differences in wind speed for each event. The average mass fluxes for each plot and each event are illustrated in table 5.

Fig. 6 shows the relation between the model prediction of spatial mass fluxes (using the calibration results) and the observed mass fluxes for 20 wind events at six the measurement plots.

The correlation between measured and predicted mass fluxes for Mugherat A and Serdah C is rather high comparing with other plots. However, correlation between the measured and predicted mass fluxes for the Serdah A and Mugherat NA measurement plots were quite poor. Proper measurement of mass flux is hampered by the occurrence of dust devils which result in an overestimation by

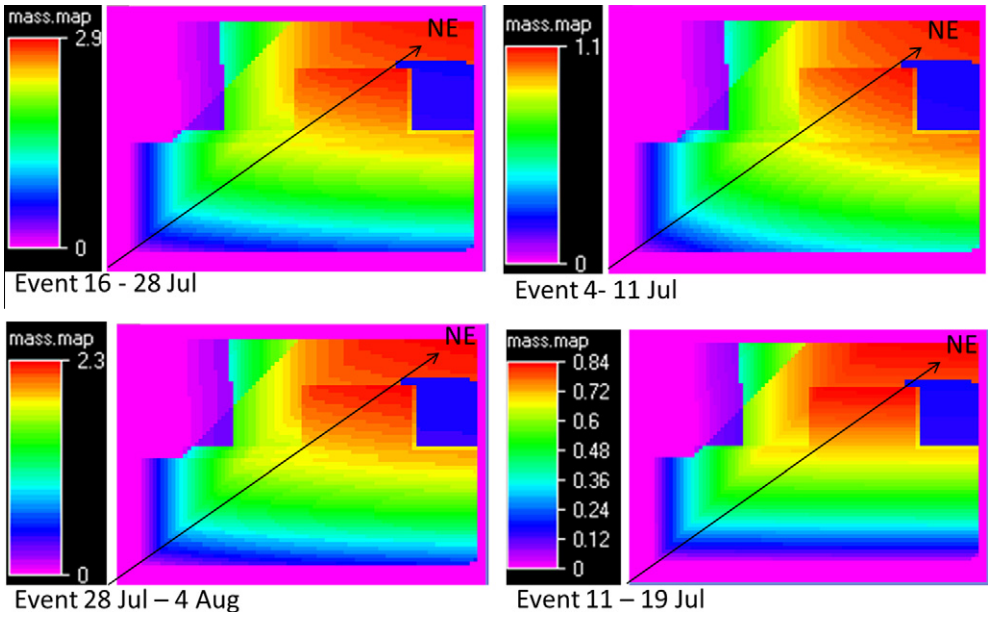

Fig. 5. Spatial distribution of the predicted total mass flux (kg m^{-1}) by the model for all wind events of Um Mial measurement plot in Khanasser valley, Syria.

Table 5
The average mass transport calculated by the model for the six measurement plots.

Site	Date	Wind factor $(m/s)^3$	$Q(x)$ average (kg m^{-1})		$Q'(x)$ average (g cm^{-1} day^{-1})[a]	
			Each event	Average	Each event	Average
Serdah A	9–30 July	114.81	0.017	0.21646	0.008	0.31540
	30 July–6 August	386.39	0.148		0.246	
	6–13 August	12.32	0.484		0.692	
Serdah C	16–28 July	177.49	0.840	2.02918	0.700	2.77383
	28 July–4 August	132.59	0.669		0.956	
	4–11 August	53.03	3.785		5.407	
	11–18 August	30.72	2.823		4.033	
Mugherat A	13–20 August	16.95	2.080	5.19967	2.971	7.42810
	20–27 August	25.41	2.790		3.985	
	27 August–3 September	102.76	10.729		15.328	
Mugherat NA	3–10 September	126.36	2.212	0.87094	3.160	1.24421
	10–18 September	13.89	0.238		0.340	
	18–25 September	9.12	0.163		0.233	
Um Mial	16–28 July	83.06	0.223	1.54977	0.186	1.964733
	28–4 August	65.70	3.682		5.260	
	4–11 August	31.51	0.744		1.240	
	11–19 August	23.73	0.821		1.173	
Adami Gazelle	9–16 September	42.30	0.685	1.57922	0.97912	2.256
	16–23 September	26.55	2.247		3.20968	
	23–30 September	6.15	1.805		2.57928	

[a] This unit g cm^{-1} day^{-1} was used to enable comparing the results of this research with results of previous studies.

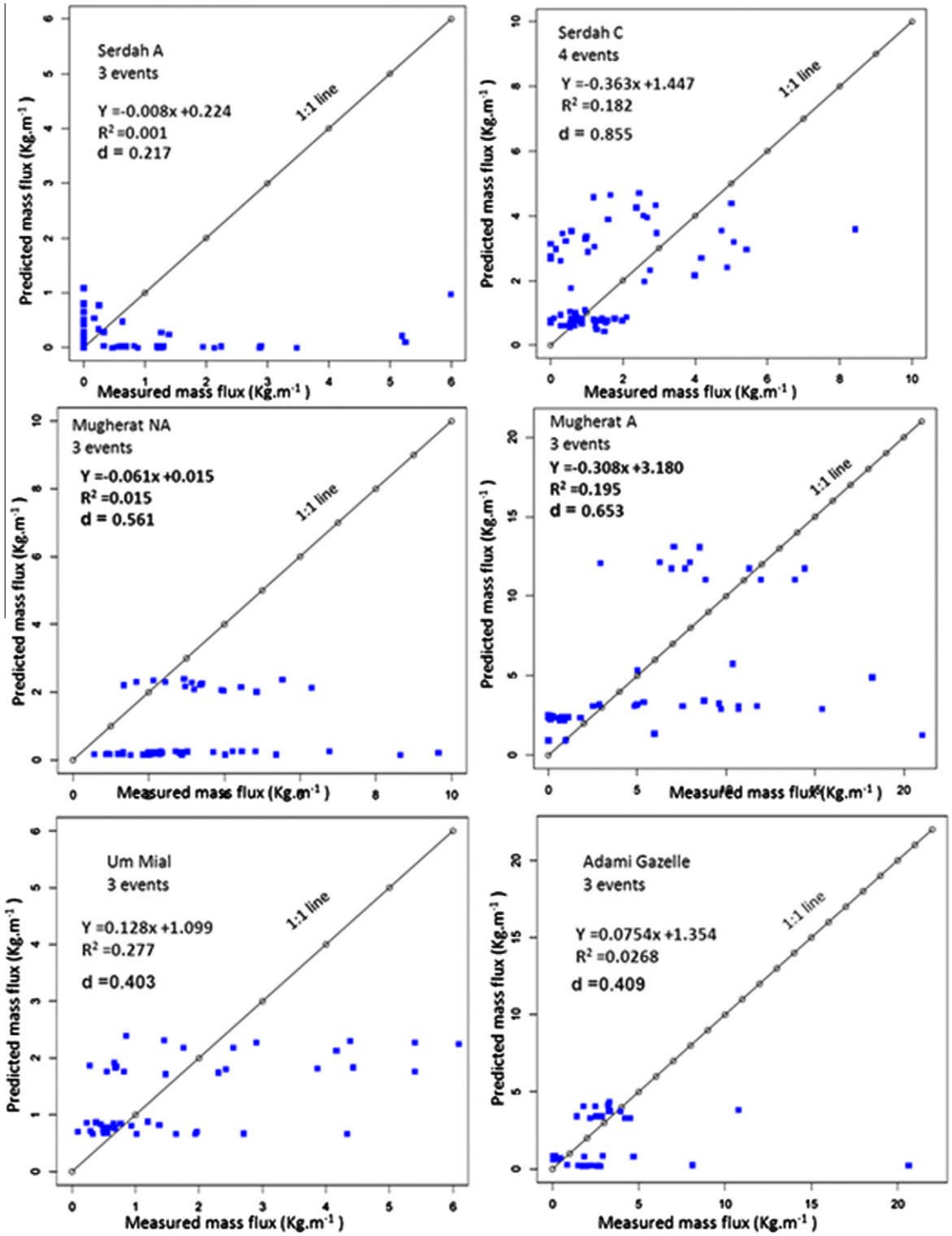

Fig. 6. Using the calibration results, the relation between the measured and predicted mass fluxes (kg m^{-1}) of every measurement plot for the full measurement time.

the measurements of the real flux. Here, we did not intend to measure dust devil because it is a rather small scale process and thus, it was excluded in this research. This can be the cause of the poor correlation between observed and modelled fluxes for the Serdah A, which resulted in higher values of the measured mass flux than that predicted by the model. In addition, for the Mugherat NA plot, the poor correlation could have been due to the entrance of sheep to the plot area during the measurement time which unexpectedly accelerated the soil movement and consequently the measured mass flux. As the Mugherat NA plot was close to the settlement, it was difficult to protect the plot from grazing during the measurement period.

The averages of measured and predicted mass fluxes over the plot are shown in Fig. 7. The correlation between the measured and predicted mass fluxes was acceptable due to the number of processes and parameters employed in the model script. As it is

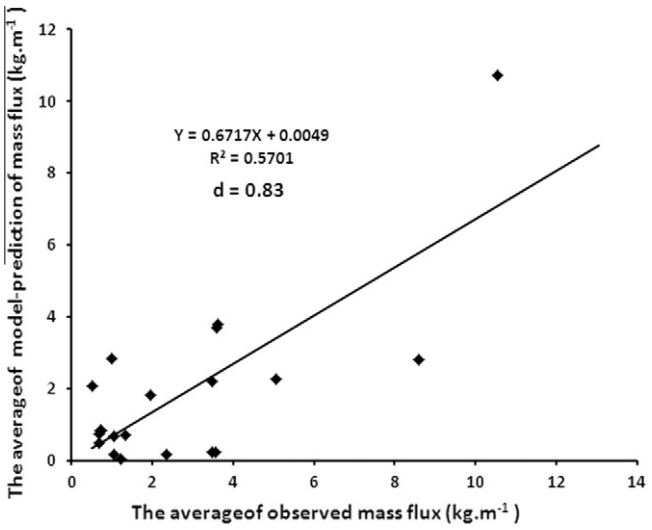

Fig. 7. Using the calibration results, the relation between the average values of the measured and predicted mass fluxes by the model (kg m^{-1}).

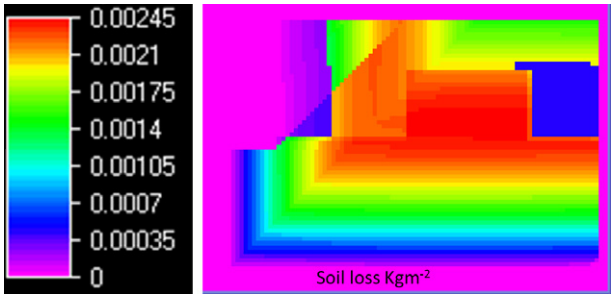

Fig. 8. The soil loss map of Um Mial plot and surrounding area for the wind event of 11–19 of August, 2009.

Table 6
The average soil loss (g m^{-2}) calculated by the model for the six measurement plots.

Site	Date	Soil loss (g m^{-2})	
		Each event	Average
Serdah A	9–30 July	0.380	0.565
	30 July–6 August	1.270	
	6–13 August	0.045	
Serdah C	16–28 July	11.920	6.402
	28 Jul–4 August	8.920	
	4–11 August	2.620	
	11–18 August	2.150	
Mugherat A	13–20 August	7.110	18.490
	20–27 August	9.610	
	27 August–3 September	38.750	
Mugherat NA	3–10 September	7.530	2.936
	10–18 September	0.760	
	18–25 September	0.520	
Um Mial	16–28 July	7.270	4.505
	28-4 August	5.880	
	4–11 August	2.610	
	11–19 August	2.260	
Adami Gazelle	9–16 September	0.740	5.63
	16–23 September	13.540	
	23–30 September	2.610	

clearly shown in Fig. 7, the correlation between measured and predicted mass fluxes was improved after averaging over the plot. This improvement of correlation when averaging the mass flux over the plot can be related to the reduction of the value of the standard deviation due to the decreasing of the number of points located far from the correlation line. These results indicated that there is the possibility of applying the average of model outputs (Bierkens et al., 2000) for upscaling the model. Upscaling the model to a regional scale was planned to be the next step of this research.

3.3. Outputs of the calibrated RWEQ

3.3.1. Mass transport

Table 5 illustrates the average mass transport $Q(x)$ (kg m^{-1}) and $Q'(x)$ (g cm^{-1} day^{-1}) calculated by the model (Eq. 1) for each wind event and the mean values of mass transport at the six measurement plots over the full measurement period (which was 3 weeks for most of the plots). It is notable in that there are differences in the predicted mass fluxes among plots and also among the events for each plot. It can be seen that the highest average mass flux for three weeks was at Mugheart A plot (5.19 kg m^{-1}). The high wind speed recorded over short time during the measurement periods was the principal cause. For example, during the wind events of 27 August–3 September, for one time step of 6 h the average wind speed was 8.97 m s^{-1}, causing a total mass flux around 5 kg m^{-1} over the simulated unit. The minimum average mass flux at the Serdah A measurement plot was 0.21 kg m^{-1}, and was linked to the well vegetated surrounding area and the high amount of residues on the soil surface. While comparing the results of this research with those obtained by ICARDA 2003 in the Khanasser valley region (Masri et al., 2003), our results show a higher mass flux. The mass transport in the region varied from 0.078 to 0.334 g cm^{-1} day^{-1} in the results of ICARDA while the measured mass flux was between 0.59 and 10.54 g cm^{-1} day^{-1} in the current study and the model predicted the mass transport was from 0.008 up to 15.32 g cm^{-1} day^{-1}. The lower mass transport of the research done by ICARDA was because they used a measurement period of 12 weeks when computing the mass flux at one plot. In the calculation of mass transport it is essential to use the event time with units of kg m^{-1} or g cm^{-1} (Sterk and Raats, 1996). In the current research the exact time of saltation was obtained through the use of a saltiphone that recorded the saltation period correctly. Thus, only saltiphone-recorded periods were used when calculating the mass fluxes.

3.3.2. Soil loss

Using the calibrated model the soil loss from each measurement plot was calculated. The spatial distribution of the net soil loss (kg m^{-2}) from the Um Mial measurement plot for the event of 11–19 August is given as an example of this calculation (Fig. 8). Table 6 gives the average net soil loss from the six measurement plot at 20 wind events.

The model results of net soil loss show that the values fluctuate among the plots and among the wind events at each plot (Table 5). Parallel to results of mass fluxes, the highest soil loss was predicted at the plot of Mugherat A with a value of 18.490 g m^{-2} (Table 6) for the average of three wind events. The minimum soil loss was predicted at the Serdah A measurement plot with a value of 0.565 g m^{-2}. Moreover, among wind events, the minimum value of soil loss was predicted for the event of 6–13 August at Serdah A with value of 0.045 g m^{-2} and the maximum value was predicted for the event of 27 August–3 September at Mugherat A with value of 38.75 g m^{-2}.

4. Conclusion

In this study, the RWEQ wind erosion model was adjusted and calibrated against ground data collected from six simulated units in stabilization zones 4 and 5 in Khanasser valley, Syria.

The original RWEQ model was mainly created to estimate the soil loss from agricultural filed in the USA. It considers the simulated unit to be homogenous, and that it has clear no-eroded borders and it uses the average of weather data over a period of 1–15 days. These specific conditions do not exist in the area used for this study. Moreover, the weather parameters change continually in the region examined, thus, averaging over such a long period may result in unrepresented parameters for weather characteristics. Therefore, adjustments to the original RWEQ model were applied in the current study. The adjustments include the simulation of sediment flux over the field boundaries and the time step which was narrowed to 6 h. This allowed the adjusted model to calculate the mass transport depending on weather inputs over these 6 h.

Mass fluxes were observed using 16 MWAC catchers on a grid set-up on a 60×60 m plot.

The weather, soil, vegetation and roughness are the main factors of the RWEQ model, and because of that, one parameter from each of these factors was calibrated using the extensive brute force calibration technique. Six calibration parameters, which were included in the determination of the critical field length (S, m), the threshold wind velocity (U_t, m s^{-1}), the erodible fraction (E_F), the crop canopy (S_{LRC}) and the soil roughness factor (K_{tot}), were used in this calibration.

With the calibrated model it is possible to calculate the mass transport and the net soil loss from simulated area units. The model results were tested against ground data collected from the study area. The results of this test showed that the coefficient of determination for the linear regression equation between measured and predicted average mass fluxes by the model at the simulated units at 20 wind events was ($R^2 = 0.57$, $d = 0.83$). This correlation is acceptable comparing with previous tests of the RWEQ model. Finally, we realize that for regional scale modelling it is important to calculate total soil loss over a plot. This was the reason behind aggregating model results over each simulated unit to calculate total soil loss using the RWEQ in PCRaster.

Acknowledgements

We would like to thank the people at both the International Center for Agricultural Research in the Dry Areas: ICARDA, Aleppo, Syria and the Branch of the General Commission of Badia Management and Development in Aleppo for their supports to complete the field measurements of this research. We also acknowledge and thank the Scientific and Technological Research Council of Turkey TUBITAK for the fellowship to the corresponding author. Finally we would like to thank two anonymous reviewers for their valuable remarks on the article.

References

Bierkens, M.P., Finke, P., Willigen, D.P., 2000. Upscaling and downscaling methods for environmental research, Kluwer, Dordrecht/Boston/London, vol. 88 (Developments in Plant and Soil Sciences).

Bruggeman, A., Rieser A, Asfahani J, Abou Zakhem, B., L.E., 2008 (Eds.), Water Resources and Use of the Khanasser Valley, ICARDA, Aleppo, Syria, International Center for Agricultural Research in the Dry Areas, Aleppo, Syria (complated report).

Buschiazzo, D.E., Zobeck, T.M., 2008. Validation of WEQ, RWEQ and WEPS wind erosion for different arable land management systems in the Argentinean Pampas. Earth Surface Processes and Landforms 33 (12), 1839–1850.

Cook, B.I., Miller, R.L., Seager, R., 2008. Dust and sea surface temperature forcing of the 1930's 'Dust Bowl' drought. Geophysical Research Letters, 35.

Copeland, N.S., Sharratt, B.S., Wu, J.Q., Foltz, R.B., Dooley, J.H., 2009. A wood-strand material for wind erosion control: effects on total sediment loss, PM10 vertical flux, and PM10 loss. Journal of Environmental Quality 38 (1), 139–148.

De Longueville, F., Henry, S., Ozer, P., 2009. Saharan dust pollution: implications for the Sahal? Epidemiology 20 (5), 780.

Feng, G., Sharratt, B., 2007. Predicting wind erosion and windblown dust emissions at the regional scale to guide strategic conservation targeting. Journal of Soil and Water Conservation 62 (5).

Fryrear, D.W. et al., 1998. Revised Wind Erosion Equation (RWEQ). Wind Erosion and Water Conservation Research Unit, Technical Bulletin 1, Southern Plains Area Cropping Systems Research Laboratory, USDA-ARS.

Hagen, L.J., 2004. Evaluation of the wind erosion prediction system (WEPS) erosion submodel on cropland fields. Environmental Modelling and Software 19 (2), 171–176.

ICARDA, 2005. Sustainable Agricultural Development for Marginal Dry Areas Khanasser Valley Integrated Research Site. International Center for Agricultural Research in the Dry Areas: Agriculture, Research, Training and Publications (ICARDA, 2005) 1.

Karssenberg, D., De Jong, K., 2005. Dynamic environmental modelling in GIS: 2 modelling error propagation. International Journal of Geographical Information Science 19 (6), 623–637.

Leenders, J.K., van Boxel, J.H., Sterk, G., 2005. Wind forces and related saltation transport. Geomorphology 71 (3-4), 357–372.

Masri, Z., Zlobisch, M., Bruggeman, A., Hayek, P., Kardous, M., 2003. Wind erosion in a marginal Mediterranean dryland area: a case study from the Khanasser Valley, Syria. Earth Surface Processes and Landforms 28 (11), 1211–1222.

Papadimitriou, F., Mairota, P., 1996. Spatial scale-dependent policy planning for land management in Southern Europe. Environmental Monitoring and Assessment 39 (1-3), 47–57.

Saleh, A., 1993. Soil roughness measurement – chain method. Journal of Soil and Water Conservation 48 (6), 527–529.

Shao, Y., Leslie, L.M., 1997. Wind erosion prediction over the Australian continent. Journal of Geophysical Research D: Atmospheres 102 (25), 30091–30105.

Spaan, W.P., van den Abeele, G.D., 1991. Wind borne particle measurements with acoustic sensors. Soil Technology 4 (1), 51–63.

Sterk, G., Raats, P.A.C., 1996. Comparison of models describing the vertical distribution of wind-eroded sediment. Soil Science Society of America Journal 60 (6), 1914–1919.

Sterk, G., Spaan, W.P., 1997. Wind erosion control with crop residues in the Sahel. Soil Science Society of America Journal 61 (3), 911–917.

Sterk, G., Herrmann, L., Bationo, A., 1996. Wind-blown nutrient transport and soil productivity changes in Southwest Niger. Land Degradation and Development 7 (4), 325–335.

Stroosnijder, L., 2007. Rainfall and land degradation in Sivakumar, In: M.V.K., N. Ndiang'ui (Eds.), Climate and land degradation. Springer, pp. 167–195.

Thomas, R.J., Turkelboom, F., 2008. An integrated livelihoods-based approach to combat desertification in marginal drylands. In: Lee, C., Schaaf, T. (Eds.), Future of Drylands, Springer, Dordrecht, pp. 631–646.

United State Department Of Agriculture, Natural Resources Conservation Service (NRCS), 2010. <http://soils.usda.gov/technical/aids/investigations/texture/>.

Van Pelt, R.S., Zobeck, T.M., Potter, K.N., Stout, J.E., Popham, T.W., 2004. Validation of the wind erosion stochastic simulator (WESS) and the revised wind erosion equation (RWEQ) for single events. Environmental Modelling and Software 19 (2), 191–198.

Visser, S.M., Sterk, G., 2007. Nutrient dynamics – wind and water erosion at the village scale in the Sahel. Land Degradation and Development 18 (5), 578–588.

Walkley, A., Black., I.A., 1934. An examination of the Degtjareff method for determining organic carbon in soils: effect of variations in digestion conditions and of inorganic soil constituents. Soil Science Society American Proceeding 29, 602–608. 63, 251–263..

Willmott, C.J., 1981. On the valldatlon of models. Physical Geography 2, 182–194.

Zobeck, T.M., Parker, N.C., Haskell, S., Guoding, K., 2000. Scaling up from field to region for wind erosion prediction using a field-scale wind erosion model and GIS. Agriculture, Ecosystems and Environment 82 (1-3), 247–259.